Electronic Supplementary Material (ESI)

Lattice constants-dependent anchoring effect of MXenes for Lithium-sulfur (Li-S) batteries: A DFT study

*Na Li,[a] Qiangqiang Meng,[a,b] Xiaohong Zhu,[a] Zhen Li,[a] Jiale Ma,[a] Changxiong Huang,[a] Jun Song,[c] and Jun Fan [a,d] **

[a] Department of Materials Science& Engineering, City University of Hong Kong, Hong Kong, China
[b] Key Laboratory for Advanced Technology in Environmental Protection of Jiangsu Province, Yancheng Institute of Technology, Yancheng, Jiangsu 224051, China.
[c] Mining and Materials Engineering, McGill University, Montreal, QC H3A 0C5, Canada
[d] Center for Advance Nuclear Safety and Sustainable Development, City University of Hong Kong, Hong Kong, China

Contents:

*Corresponding author: junfan@cityu.edu.hk

SI-1: Interactions Between Soluble LiPSs and Organic Electrolyte

DOL and DME were chosen as representative molecules to investigate the interaction between LiPSs and organic electrolyte in Li-S batteries.[1-3] Optimized structures of DOL, DME and soluble LiPSs anchored on them were shown in Figure S1. We noted that the binding of Li_2S_8 and Li_2S_4 on DOL and DME comes from the interaction between Li atom of LiPSs and O atoms of organic electrolyte molecules with a length of Li-O bond around 1.90 Å. In addition, binding energy values of Li_2S_8 and Li_2S_4 on DOL and DME were in the range of 0.77-0.87 eV. Furthermore, we also calculated the binding energies of Li_2S_8 and Li_2S_4 over Ti_2CO_2 with the co-existence of DOL and DME on Ti_2CO_2. As shown in Figure S2, the existence of DOL and DME has enhanced the binding energies of Li_2S_8 and Li_2S_4 on Ti_2CO_2 by 0.25 eV and 0.11 eV, respectively. These results further demonstrated the effectiveness of MXenes serving as sulfur hosts.

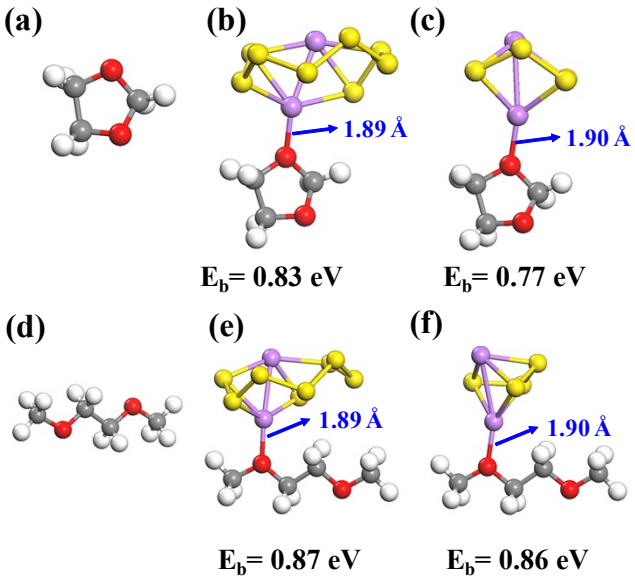

Figure S1 Optimized structures of (a) DOL; (b) Li_2S_8 anchored on DOL; (c) Li_2S_4 anchored on DOL; (d) DME; (e) Li_2S_8 anchored on DME; (f) Li_2S_4 anchored on DME. The calculated binding energies (E_b in eV) of LiPSs on two organic electrolyte molecules are also given.

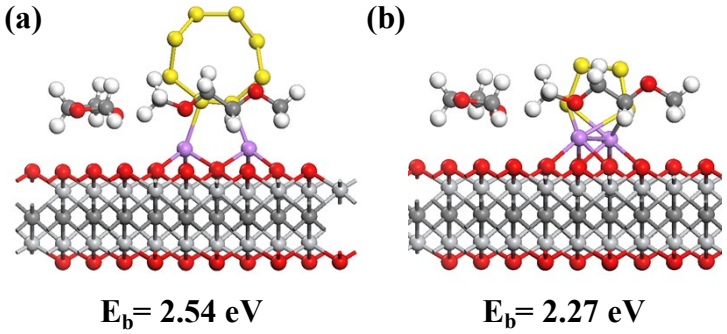

Figure S2 Optimized structures of (a) Li_2S_8, DOL and DME co-anchored on Ti_2CO_2 monolayer; (b) Li_2S_4, DOL and DME co-anchored on Ti_2CO_2 monolayer; The calculated binding energies (E_b in eV) of Li_2S_8 and Li_2S_4 on Ti_2CO_2 monolayer coexisted with two organic electrolyte molecules are also given.

SI-2: Confirmation of the Most Favorable Adsorption Configuration of Various LiPSs over Ti_2CO_2

To identify the most favorable adsorption configuration of sulfides over Ti_2CO_2, we calculated all potential adsorption configurations of Li_2S_8, Li_2S_4 and Li_2S over Ti_2CO_2. The surface of Ti_2CO_2 possesses three structurally distinct adsorption sites which are: (i) a-site on top of O atom, (ii) b-site on top of Ti atom and (iii) c-site on top of C atom. The potential adsorption configurations of LiPSs over Ti_2CO_2 can be categorized into two classes: parallel and vertical configurations. In parallel configurations, only one Li atom of LiPSs participated the interaction with the substrates while in vertical configurations both two Li atoms of LiPSs interacted with the surface of Ti_2CO_2. For all three selected LiPSs, the vertical configuration that two Li atoms of LiPSs located on top of two adjacent C atoms provided the largest E_b for its strongest interaction between Li atoms and O atoms and relatively weak repulsion between Li atoms and Ti atoms.

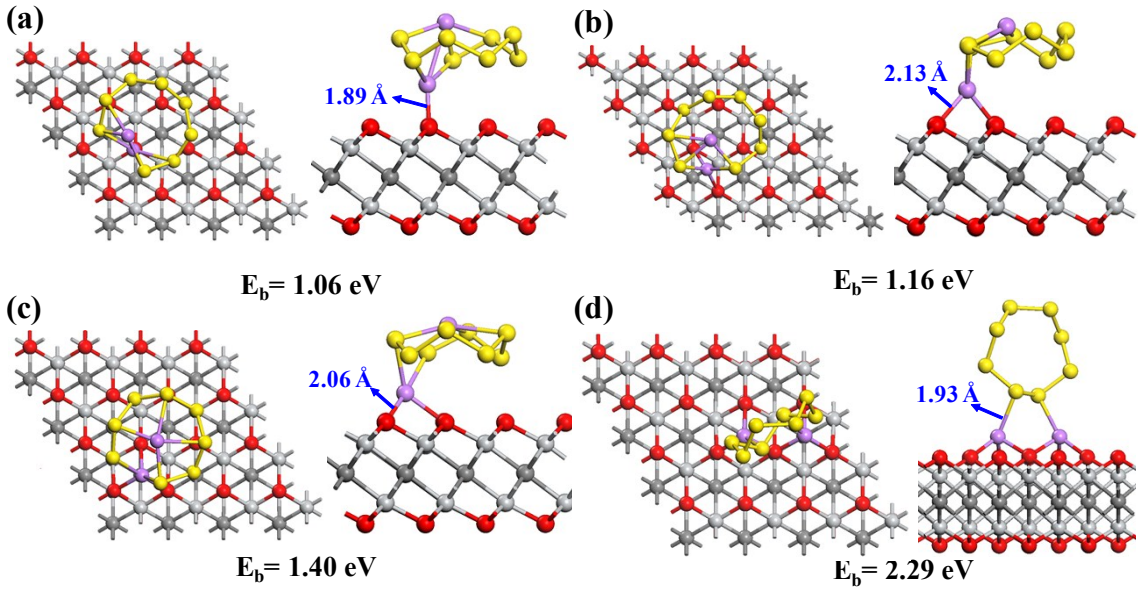

Figure S3 Confirmation of the most favorable adsorption configuration of Li_2S_8 on monolayer Ti_2CO_2. Optimized structures of potential adsorption configurations were shown in (a) to (d) and the calculated binding energies (E_b in eV) are also given

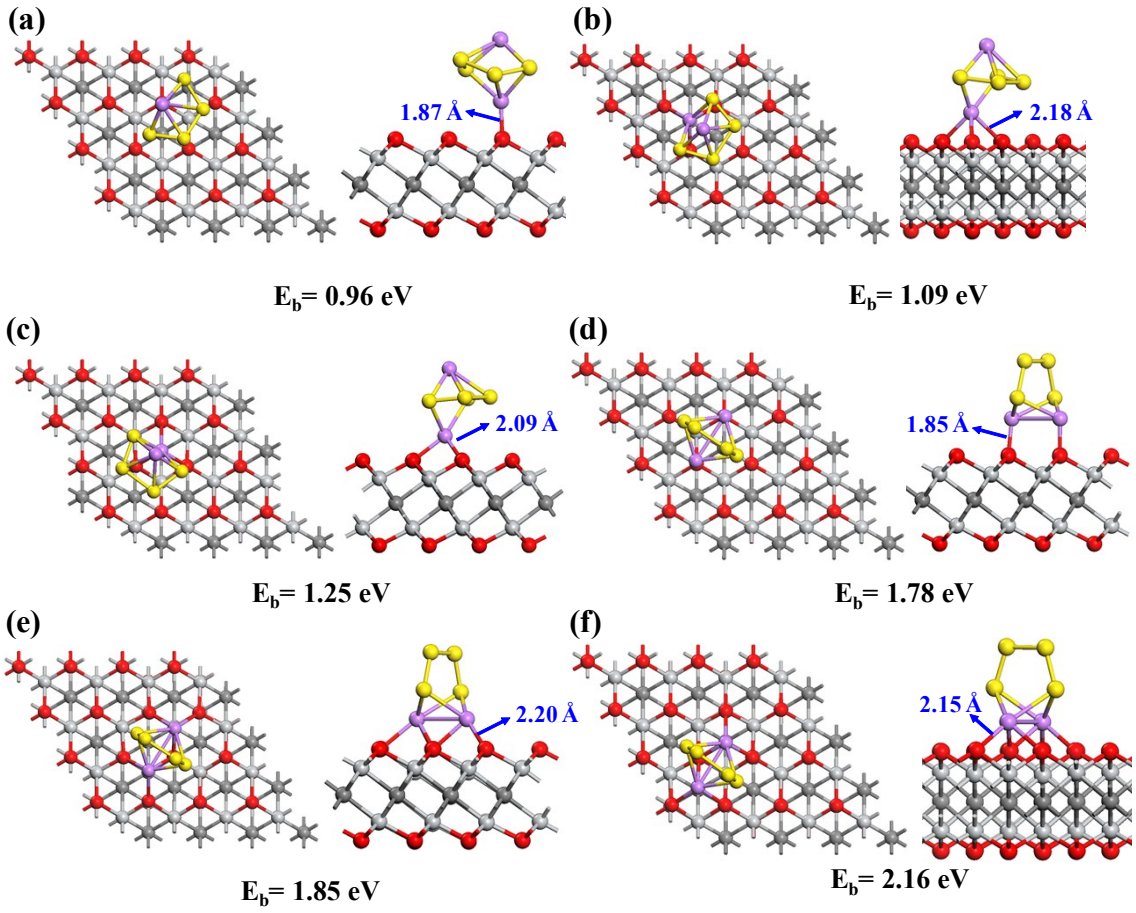

Figure S4 Confirmation of the most favorable adsorption configuration of Li_2S_4 on monolayer Ti_2CO_2. Optimized structures of potential adsorption configurations were shown in (a) to (f) and the calculated binding energies (E_b in eV) are also given.

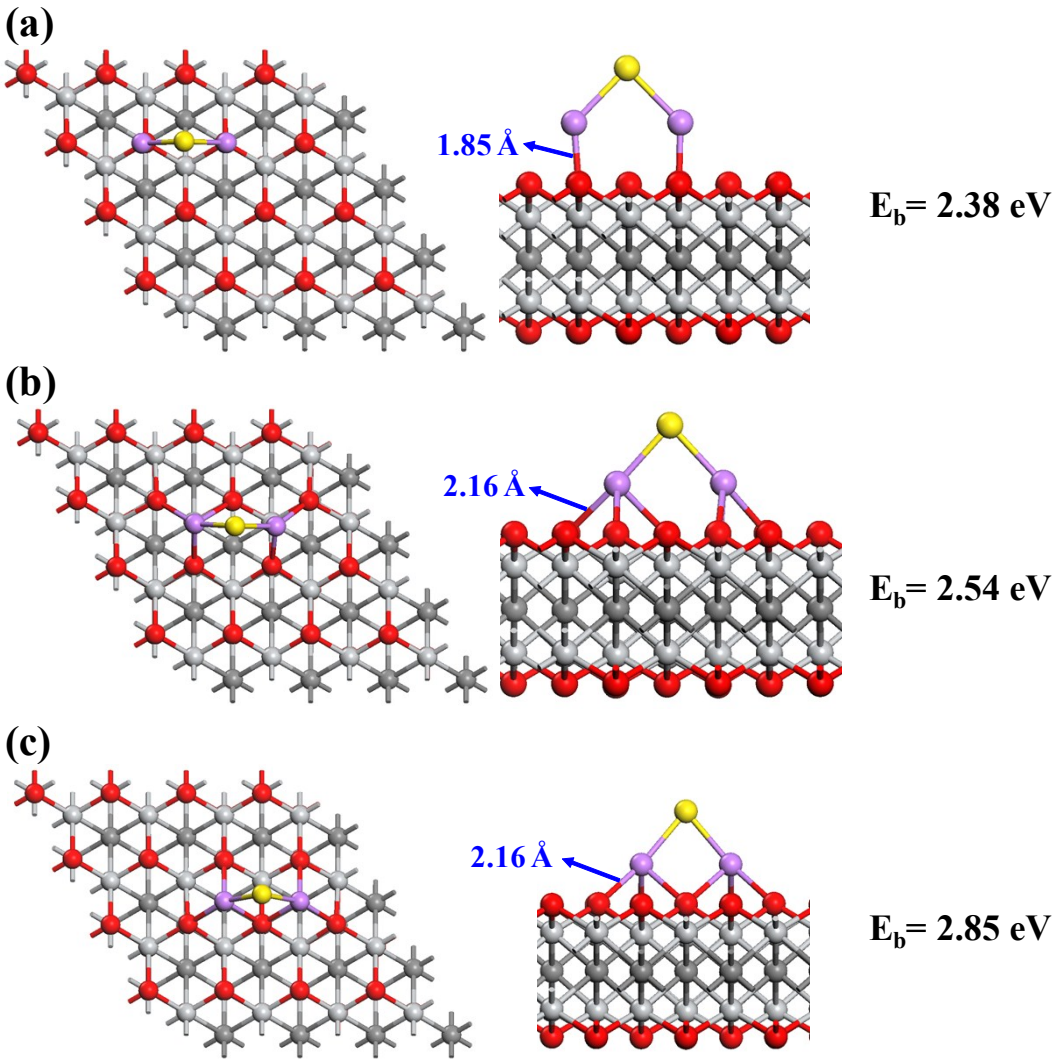

Figure S5 Confirmation of the most favorable adsorption configuration of Li_2S on monolayer Ti_2CO_2. Optimized structures of potential adsorption configurations were shown in (a) to (c) and the calculated binding energies (E_b in eV) are also given.

SI-3: Effect of the numbers of layers of MXenes on the binding energy of LiPSs over MXenes

MXenes are multilayered when used in Li-S batteries serving as sulfur host based on the SEM images. In order to efficiently investigate the mechanism at atomic scale, sometimes theoretical models are always ideal compared with experiments. To better reflect the experimental situation, it is significant to investigate the effect of the layers of MXenes on the binding energies of LiPSs. Therefore, we compared the binding energies of S_8, Li_2S_8, Li_2S_4 and Li_2S over Ti_2CO_2 monolayer with bilayer.

Specifically, binding energies of S_8, Li_2S_8, Li_2S_4 and Li_2S over Ti_2CO_2 bilayer were calculated. Based on our calculation results, the additional layer of Ti_2CO_2 has little effect on the binding energies of sulfides on MXenes. Specifically, compared to Ti_2CO_2 monolayer, binding energies of S_8 over Ti_2CO_2 bilayer decreased by 0.01 eV while Li_2S_8, Li_2S_4 and Li_2S increased by 0.13 eV, 0.09 eV and 0.05 eV.

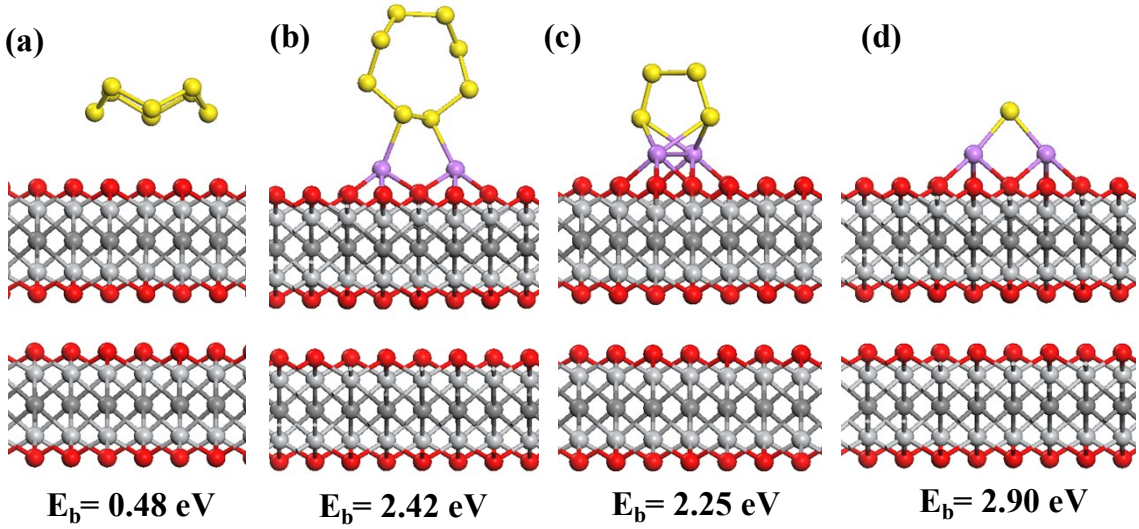

Figure S6 Optimized structures of S_8, Li_2S_8, Li_2S_4 and Li_2S anchored on Ti_2CO_2 bilayer were shown in (a) to (d) and the calculated binding energies (E_b in eV) are also given.

SI-4: Optimized Structures of Various Sulfides Anchored on $M_3C_2O_2$ (Cr, V, Nb, Hf and Zr)

Optimized structures of S_8, Li_2S_8, Li_2S_4 and Li_2S anchored on $Cr_3C_2O_2$, $V_3C_2O_2$, $Nb_3C_2O_2$, $Hf_3C_2O_2$ and $Zr_3C_2O_2$ were similar to those on Ti-based MXenes. As for S_8 molecule, the nearest distance between it and the surface of substrates were in the range of 3.07-3.29 eV, indicating the weak interaction between them. On the contrary, the interaction between LiPSs and substrates were much stronger owing to the existence of Li atoms.

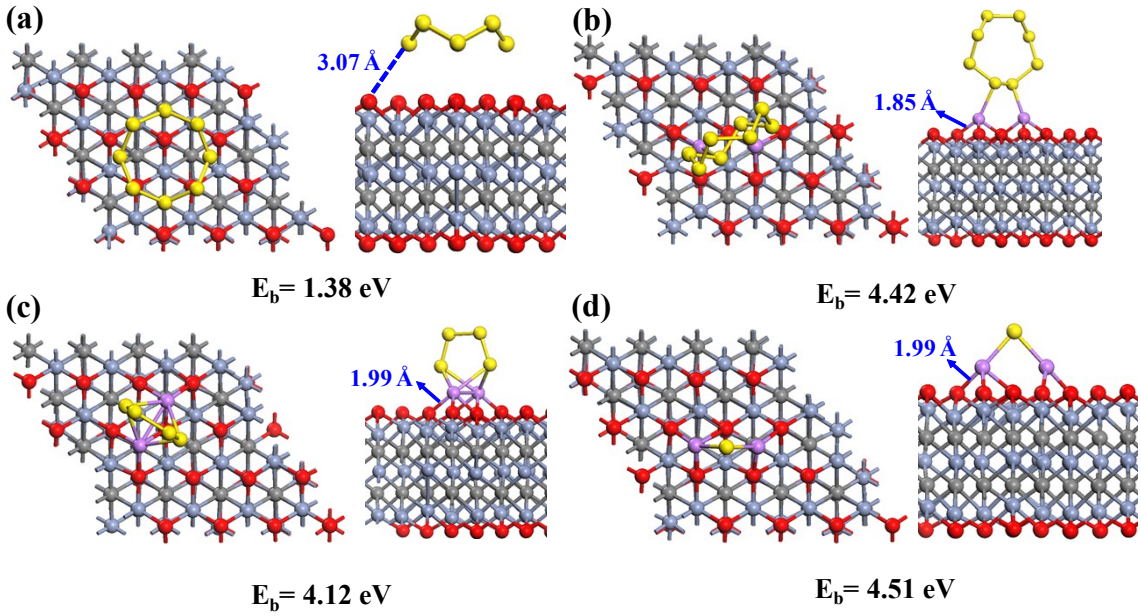

Figure S7 The most stable binding configuration of various sulfur-containing species: (a) S_8, (b) Li_2S_8, (c) Li_2S_4 and (d) Li_2S over monolayer $Cr_3C_2O_2$. Corresponding binding energies (E_b in eV) of each configuration are also given.

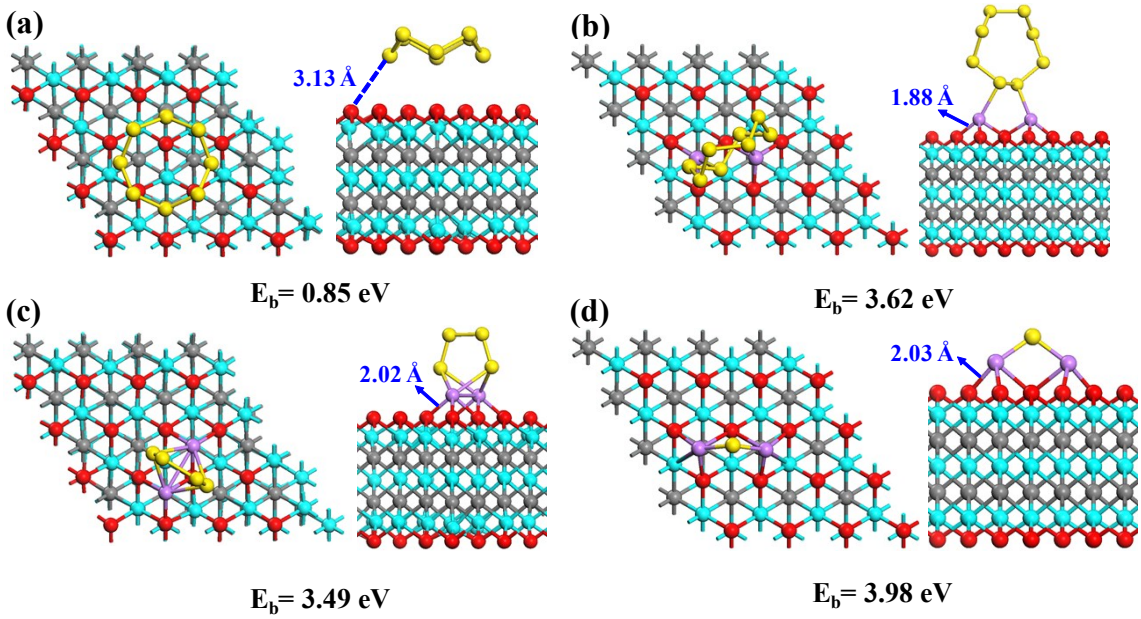

Figure S8 The most stable binding configuration of various sulfur-containing species: (a) S_8, (b) Li_2S_8, (c) Li_2S_4 and (d) Li_2S over monolayer $V_3C_2O_2$. Corresponding binding energies (E_b in eV) of each configuration are also given.

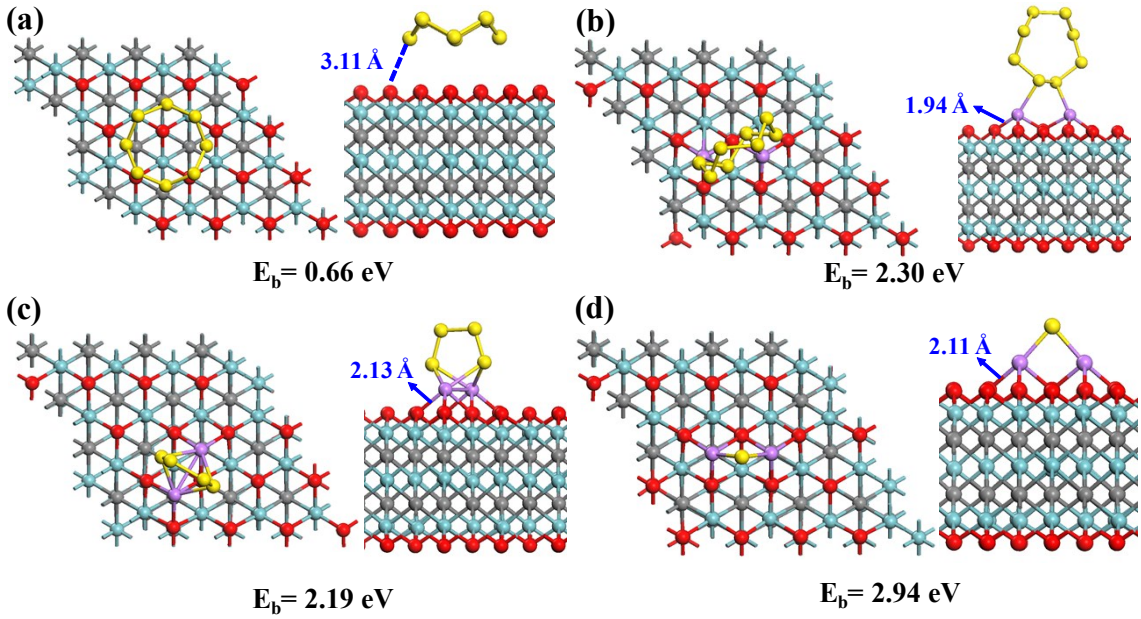

Figure S9 The most stable binding configuration of various sulfur-containing species: (a) S_8, (b) Li_2S_8, (c) Li_2S_4 and (d) Li_2S over monolayer $Nb_3C_2O_2$. Corresponding binding energies (E_b in eV) of each configuration are also given.

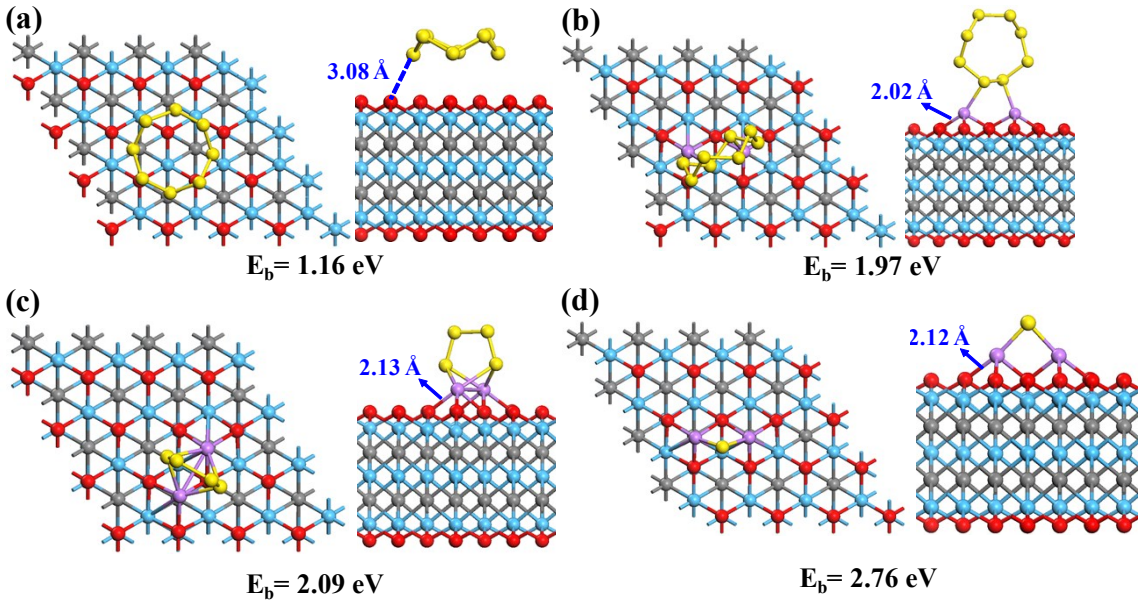

Figure S10 The most stable binding configuration of various sulfur-containing species: (a) S_8, (b) Li_2S_8, (c) Li_2S_4 and (d) Li_2S. over monolayer $Nb_3C_2O_2$. Corresponding binding energies (E_b in eV) of each configuration are also given.

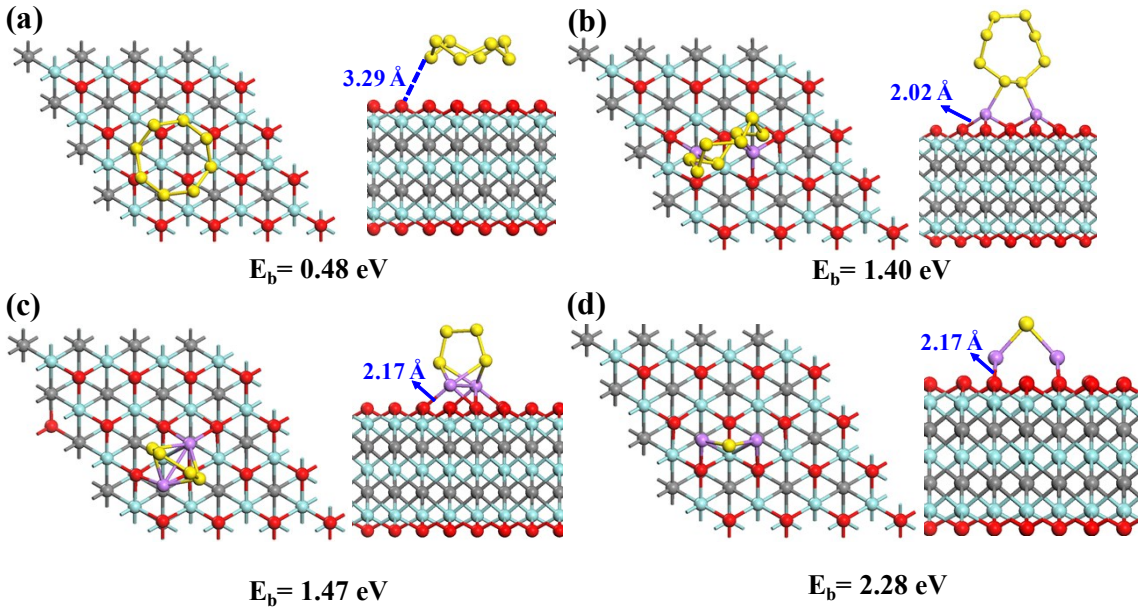

Figure S11 The most stable binding configuration of various sulfur-containing species: (a) S_8, (b) Li_2S_8, (c) Li_2S_4 and (d) Li_2S over monolayer $Zr_3C_2O_2$. Corresponding binding energies (E_b in eV) of each configuration are also given.

SI-5: Stability of the anchored Li_2S_4 on $Cr_3C_2O_2$ monolayer

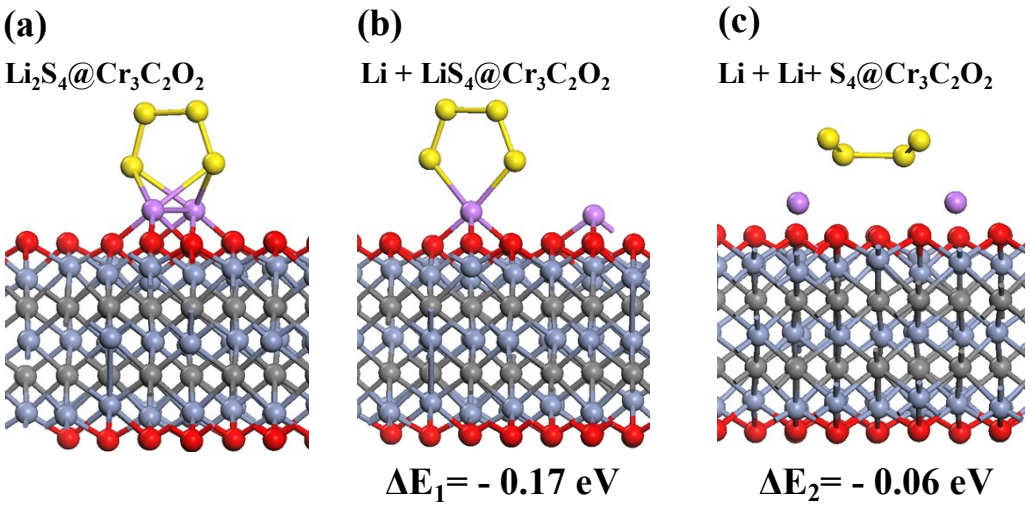

Figure S12 Atomic configurations for (a) Li_2S_4, (b) $Li+LiS_4$ and (c) $Li+Li+S_4$ clusters adsorbed on $Cr_3C_2O_2$ and their relative energy difference. Here, $\Delta E_1=E(Li_2S_4+Cr_3C_2O_2)-E(Li+LiS_4+Cr_3C_2O_2)$, and $\Delta E_2=E(Li_2S_4+Cr_3C_2O_2) - E(Li+Li+S_4+Cr_3C_2O_2)$, respectively.

SI-6: Differential Charge Density between Li_2S_4 and $M_3C_2O_2$ Surfaces

As shown in Figure S10, it is apparent that for all $Li_2S_4@M_3C_2O_2$ systems there existed a plenty of charge transfer from LiPSs to the host under the isosurface level of 0.06 e $Å^{-3}$, which manifests the strong interaction between them. Furthermore, based on the Bader charge calculation results, with the lattice constants of $M_3C_2O_2$ increased (from a to f), the number of electrons transferred obviously decreased, which is consistent with the trend of E_b values of Li_2S_4.

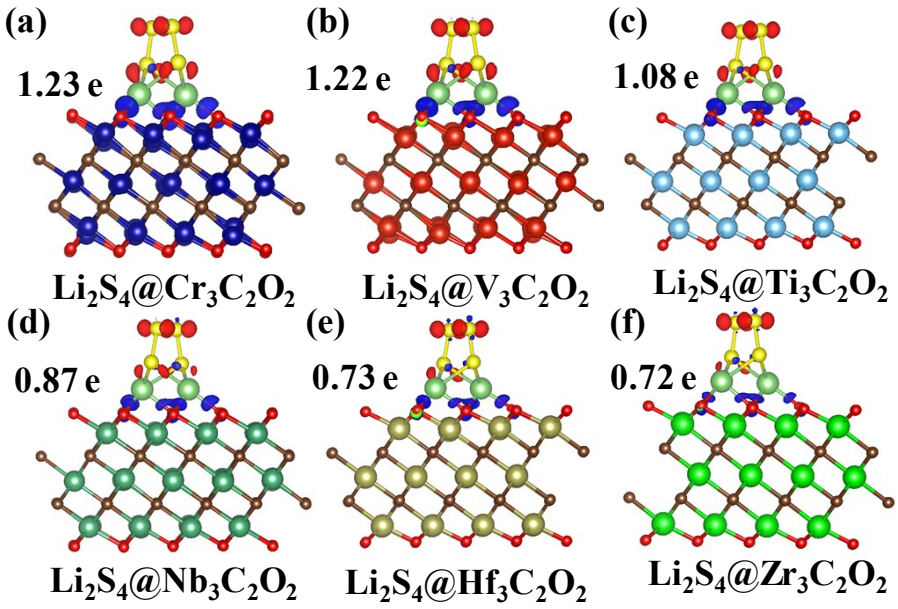

Figure S13 Differential charge density between Li_2S_4 and $M_3C_2O_2$ surfaces (a-f: $Cr_3C_2O_2$, $V_3C_2O_2$, $Ti_3C_2O_2$, $Nb_3C_2O_2$, $Hf_3C_2O_2$ and $Zr_3C_2O_2$). The isosurface level is set to be 0.06 e $Å^{-3}$. Blue and red regions indicate charge accumulation and depletion, respectively. Bader charge numbers indicate the magnitude of electrons transferred from the LiPSs to the host material.

SI-7: Density of states (DOS) of $M_3C_2O_2$ MXenes and Selected LiPSs Adsorbed Samples

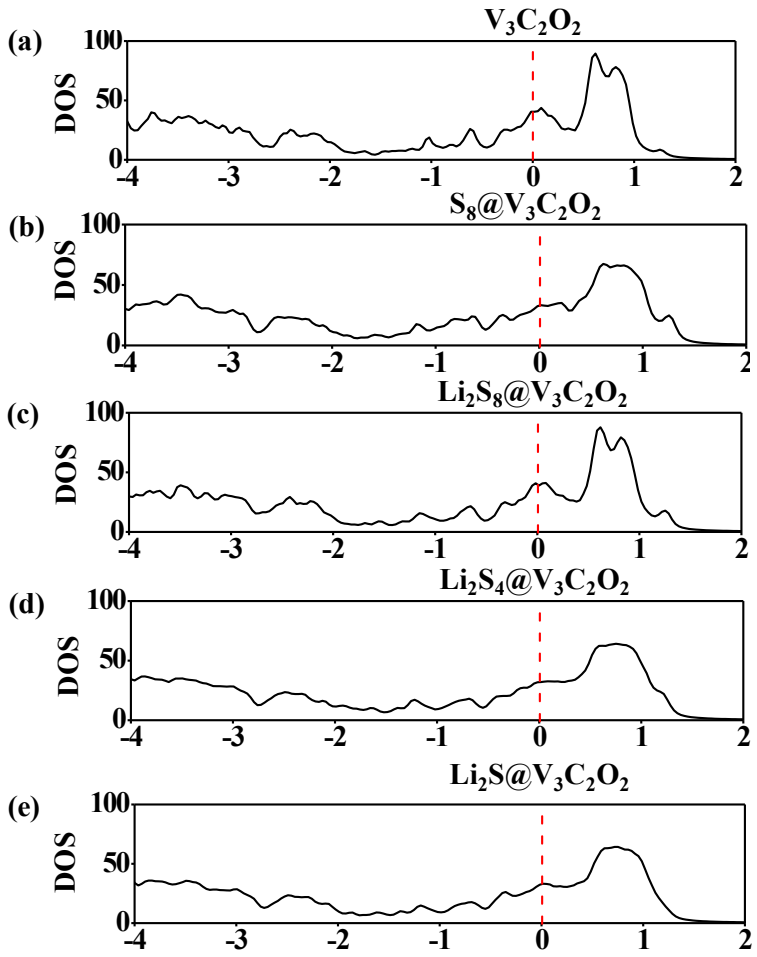

Figure S14 Density of states (DOS) of $V_3C_2O_2$ MXenes and selected LiPSs adsorbed samples.

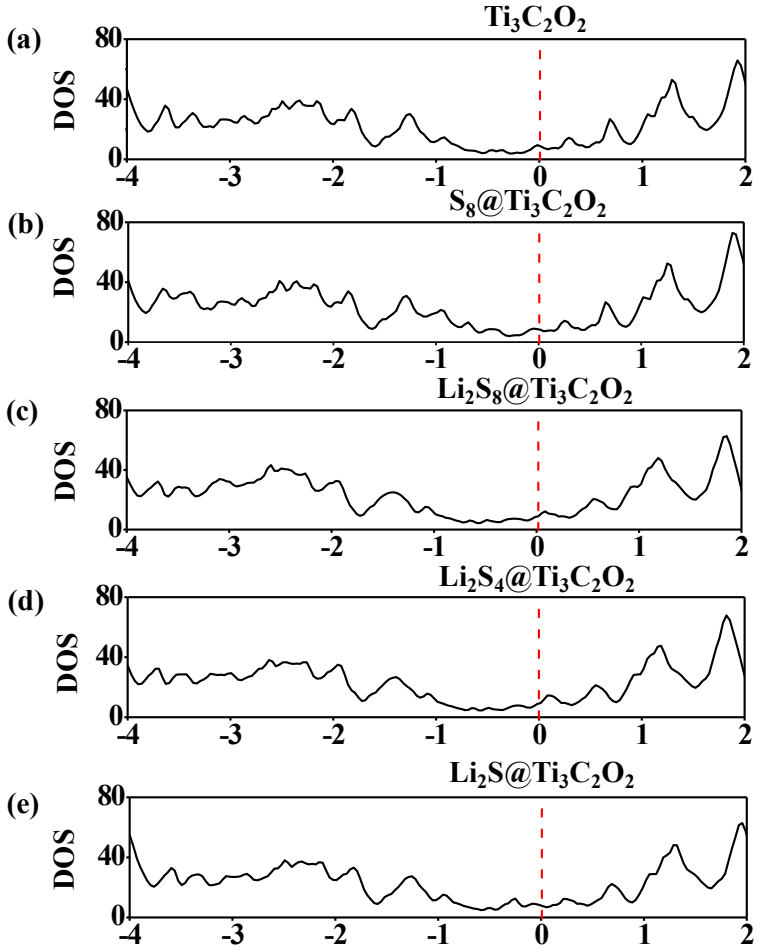

Figure S15 Density of states (DOS) of $Ti_3C_2O_2$ MXenes and selected LiPSs adsorbed samples.

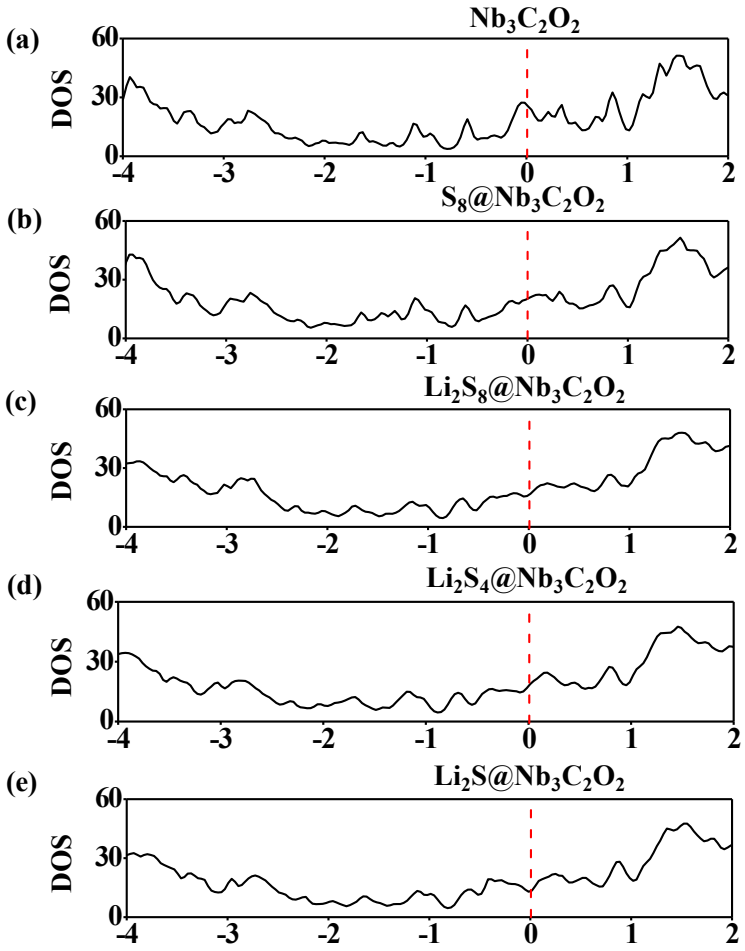

Figure S16 Density of states (DOS) of $Nb_3C_2O_2$ MXenes and selected LiPSs adsorbed samples.

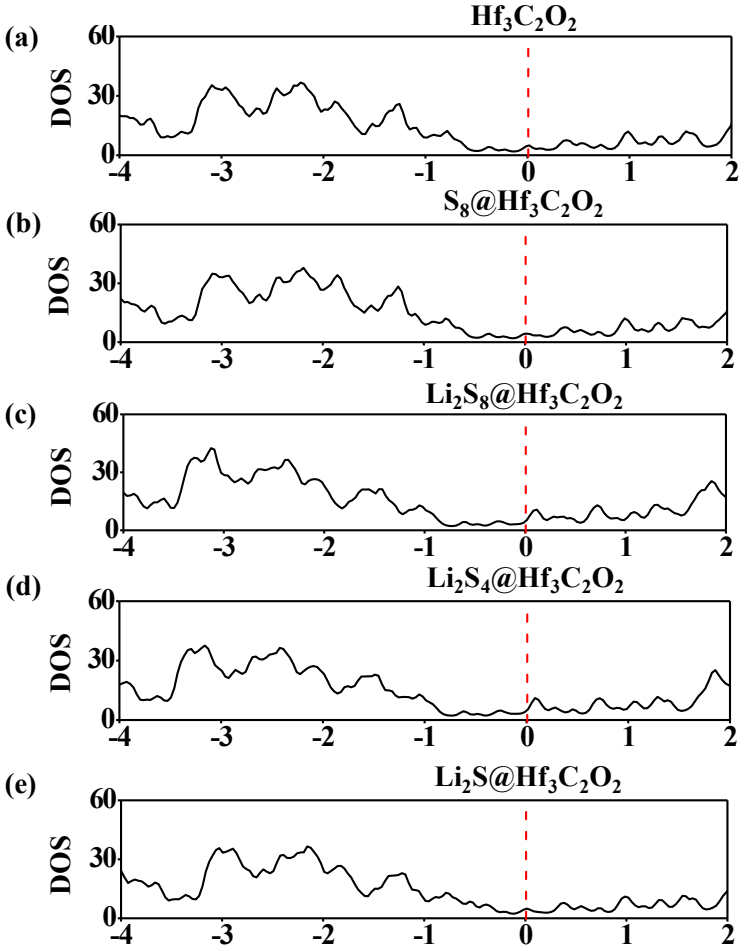

Figure S17 Density of states (DOS) of $Hf_3C_2O_2$ MXenes and selected LiPSs adsorbed samples.

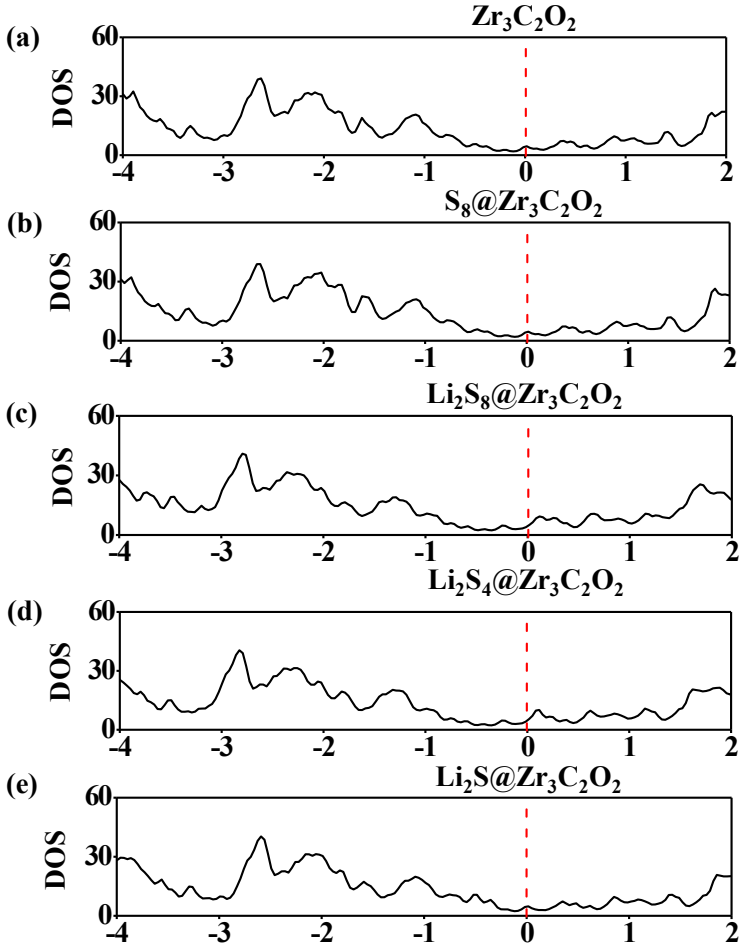

Figure S18 Density of states (DOS) of $Zr_3C_2O_2$ MXenes and selected LiPSs adsorbed samples.

References

1. L.-C. Yin, J. Liang, G.-M. Zhou, F. Li, R. Saito and H.-M. Cheng, *Nano Energy*, **2016**, 25, 203-210.
2. D. Rao, L. Zhang, Y. Wang, Z. Meng, X. Qian, J. Liu, X. Shen, G. Qiao and R. Lu, *The Journal of Physical Chemistry C*, **2017**, 121, 11047-11054.
3. E. S. Sim, G. S. Yi, M. Je, Y. Lee and Y.-C. Chung, *Journal of Power Sources*, **2017**, 342, 64-69.